
PROGNOSTIC POWER OF TEXTURE BASED MORPHOLOGICAL OPERATIONS IN A RADIOMICS STUDY FOR LUNG CANCER

A PREPRINT

Paul Desbordes
ICTEAM
Université catholique de Louvain
Louvain-la-Neuve, Belgium
paul.desbordes@uclouvain.be

Diksha
Indian Institute of Technology Ropar
Punjab, India
2016eeb1074@iitrpr.ac.in

Benoit Macq
ICTEAM
Université catholique de Louvain
Louvain-la-Neuve, Belgium
benoit.macq@uclouvain.be

December 24, 2020

ABSTRACT

The importance of radiomics features for predicting patient outcome is now well-established. Early study of prognostic features can lead to a more efficient treatment personalisation. For this reason new radiomics features obtained through mathematical morphology-based operations are proposed. Their study is conducted on an open database of patients suffering from Nonsmall Cells Lung Carcinoma (NSCLC). The tumor features are extracted from the CT images and analyzed via PCA and a Kaplan-Meier survival analysis in order to select the most relevant ones. Among the 1,589 studied features, 32 are found relevant to predict patient survival: 27 classical radiomics features and five MM features (including both granularity and morphological covariance features). These features will contribute towards the prognostic models, and eventually to clinical decision making and the course of treatment for patients.

Keywords Radiomics · Mathematical morphology-based features · NSCLC

1 Introduction

Radiomics is a fast-growing concept that aims for high-throughput extraction and analysis of large amounts of quantitative features from clinical images [1]. Advanced analysis can reveal the prognostic and the predictive power of features which helps avoid invasive exams while improving the treatment decisions and the likely course of the disease for the patient. Several articles can already be found in the literature. In this article, we focus on lung cancer examined by CT images which are particularly interesting to reveal the high-density contrast between tumor and lungs, as well as the intra-tumor textures and the tumor shape.

In [4], Aerts et al. studied the relevance of 440 radiomics features extracted from CT of 1,019 patients with head and neck cancer (H&N) and NonSmall Cell Lung Carcinoma (NSCLC). It revealed that a large number of them have a prognostic power ($p > 5\%$). By combining four of them, the prognostic performance was slightly higher than TNM stage or tumor volume that are the references in this kind of study. This signature, capturing intra-tumor heterogeneity, was validated latter by Leijenaar et al. [5] on a cohort of patients suffering from oro-pharyngeal squamous cell carcinoma. In [6], Aerts et al. investigated the relevance of CT radiomics features to predict mutations status in NSCLC. From their study, one radiomics feature (laws-energy) appeared to be significantly predictive of this mutation ($AUC = 0.67$, $p = 0.03$) whereas the tumor volume is not ($p > 5\%$). Other studies have shown the importance of radiomics features in predicting pathological response prior to surgery [7], for response assessment following ablative radiotherapy for early stage NSCLC [8] and for estimating disease-free survival in patients with early-stage NSCLC [9].

The Image Biomarker Standardisation Initiative (IBSI) proposed recommendations to standardise the radiomics process [10], especially promoting features with best reproducibility. Despite a controlled protocol, conclusions about radiomics features varied from a study to another. Ger et al. [11] retrospectively studied the prognostic power PET/CT features from a large cohort of H&N cancer patients. They found a higher Area Under the Curve (AUC) when studying tumor

volume alone rather than its combination radiomics features meaning they are not consistently associated with survival in CT or PET images of H&N patients, even with the same protocol.

With the aim of finding new relevant features quantifying medical images in a reproducibility way, we propose to study Mathematical Morphology (MM) based features. MM provides a very rich variety of texture descriptors that benefit from its shape-based nature and its capacity to exploit the spatial relationships among pixels [12]. High classification performances have been observed in various fields of image processing such as automatic recognition of cancerous tissues based on cells analysis using microscopic images [13], image enhancement [14] and extraction of numerical features from solar images [15]. Aptoula et al. [12] suggested that these interesting results are obtained thanks to the capacity of morphological series to capture higher order properties of spatial random processes without being limited by the theoretical bounds imposed on alternative approaches. Despite these interesting results, MM features have never been studied, to our knowledge, in a radiomics context.

In this paper we propose to study the prognostic power of features extracted with MM tools. For that, a radiomics study is performed using an open access medical images dataset composed of patients suffering from lung cancer [16]. A Kaplan-Meier survival analysis is performed to study the features relevance to predict Overall Survival (OS). Furthermore, MM based features are compared with classical radiomics (CR) features (first-order, shape-based and textures) to check if these new features bring new information.

2 Materials and methods

2.1 Patient population

The dataset retrospectively studied contains a total of 422 patients suffering from NSCLC [16]. The inclusion criteria for our study are the availability of a chest CT exam performed before the treatment, a manual segmentation of the tumor performed by an expert and the integrity of the clinical data. As a result, the dataset shrank from 422 to 297 patients. Several clinical and demographic features of these patients are summarized in Table 1.

CT images were acquired using different devices from Siemens Healthcare (Biograph 40, Sensation 10, Sensation 16 and Sensation Open) and using different parameters. Because of the variability of voxels resolution and according to the ISBI recommendations [10], a resampling step is performed to reach a spacing of $1 \times 1 \times 1 \text{ mm}^3$, which improves data homogeneity.

2.2 Feature extraction

The following workflow is performed to extract features from the CTs. The tumor volume is firstly manually segmented by experts leading to a mean tumor volume of $26.6 \pm 35.2 \text{ cm}^3$ (range: $0.2 - 263.7 \text{ cm}^3$). From this Volume-Of-Interest (VOI), two categories of features are extracted : CR and MM based features. The CR features are extracted following the ISBI protocol leading to ten first-order features, one shape feature and 37 texture features coming from four different texture matrices (Gray-Level Cooccurrence Matrix (GLCM), Gray-Level Run-Length Matrix (GLRLM), Gray-Level Size-Zone Matrix (GLSZM) and Gray-Level Difference Matrix (GLDM)). GLCM and GLRLM are computed in all the thirteen 3D directions (separated by 45°) within the neighborhood of Chebyshev with a distance of one. Features are then extracted from the resulting mean matrix.

For the MM based features, the methodology proposed by [12] is used. Two kinds of MM features are extracted: granularity and morphological covariance (including granularity and covariance moments). Ten successive iterations for each MM granularity feature and 130 for each MM covariance feature are performed, giving us a total of 1,550 MM based features. Here again the Chebyshev thirteen unique directions are used with a distance of one. In Table 2 are listed all the image features used in this study (49 CR features and 1550 MM features).

2.3 Statistical analysis

To keep uncorrelated features and eliminate redundant ones, a Spearman's rank correlation analysis is performed as a first step. The 1,589 features are compared one by one to bring out non-linear relationships. They are considered as significant if the absolute value of the Spearman's correlation coefficient ($|\rho|$) is higher or equal to 0.8 with a p -value smaller than 5% [17].

Next, Principal Component Analysis (PCA) is used on the MM features to reduce dimensionality by preserving most of the valuable information [18]. PCA allows us to evaluate the intra-class variability along the direction of the largest variance in the feature space. For each of the 22 MM features in Table 2, we retain 5 PCA components, since they

Table 1: List of clinical and demographic features of the 297 NSCLC patients included in our study.

Features	Number of patients
<i>Demographic</i>	
Patient's age (years)	
Median (range)	68.3 (42.5 - 91.7)
Mean (standard deviation)	68.0 (10.0)
Patient's gender	
Male	211 (71%)
Female	86 (29%)
<i>Clinical</i>	
Histology	
Adenocarcinoma	30 (10.1%)
Not otherwise specified	50 (16.8%)
Large cells	96 (32.3%)
Squamous cell Carcinoma	85 (28.6%)
Unknown	36 (12.1%)
TNM clinical stage	
I	76 (25.6%)
II	25 (8.4%)
III (a & b)	195 (65.7%)
Unknown	1 (0.3%)
<i>Outcomes</i>	
Follow-up (months)	
Median (range)	16.1 (0.8 - 71)
Mean (standard deviation)	19.5 (14.9)
Last news survival	
Alive	99 (33.3%)
Dead	198 (66.7%)
Two-years survival	
Alive	128 (43.1%)
Dead	169 (56.9%)

contain most of the information. This step leads to a selection of 49 CR and 110 MM features, for a total of 159 post-PCA features.

To assess the prognostic value of these features, a univariate Kaplan-Meier analysis is performed to estimate the survival distribution. The OS is calculated from the date of the initial diagnosis to the date of death or to the end of the follow-up period. Patients who are alive are censored at the time of the last recording. The association between OS and each feature is performed after a dichotomization process. The most discriminating cut-off value allowing the differentiation of the two groups of patients is selected using the Receiver Operating Characteristic (ROC) methodology. ROC curves led to AUC, Sensitivity (Se) and Specificity (Sp). The prognostic value of each feature is assessed using the log-rank test where a p -value less than 5% is considered to be statistically significant. The Kaplan-Meier analysis leads to median survival, percentage of deaths in each group and Hazard Ratio (HR).

To avoid false conclusions, appropriate statistical corrections for the type-I errors are performed according to Chalkidou et al. [19]. For each p -value calculated, a Benjamini-Hochberg correction for multiple hypotheses testing is applied. Furthermore, a correction of the minimal p -values obtained from the optimum cut-off approach is performed using the Altman formula [20].

3 Results

3.1 Correlation analysis

Results of the correlation study are represented Figure 1. A first focus on the 49 CR features is performed. Because, no correlation pattern appears, we chose to continue to study all of them without any PCA reduction.

In Figure 1b are represented the correlations between the 1,589 studied features (CR and MM features). Because there is no correlation pattern between CR, granularity and morphological covariance features we chose to deal with

Table 2: List of the studied image features.

Type of features	Features
First-order	Volume, Sum of intensities (I_{sum}), I_{max} , I_{min} , I_{mean} , I_{std} , I_{cov} , Skewness, Kurtosis, Energy, Entropy
Shape based	Sphericity
Radiomics textures	GLCM: Variance, Energy, Entropy, Correlation, Dissimilarity, Contrast, Homogeneity, Inverse Differential Moment (IDM), Cluster shade, Cluster tendency GLRLM: Short Run Emphasis (SRE), Long Run Emphasis (LRE), Low Gray-level Run Emphasis (LGRE), High Gray-level Run Emphasis (HGRE), Short Run Low Gray-level Emphasis (SRLGE), Long Run Low Gray-level Emphasis (LRLGE), Short Run High Gray-level Emphasis (SRHGE), Long Run High Gray-level Emphasis (LRHGE), Run Percentage (RP), Gray-level Non-Uniformity (GLNUr), Run Length Non Uniformity (RLNU) GLSZM: Short Zone Emphasis (SZE), Long Zone Emphasis (LZE), Low Gray-level Zone Emphasis (LGZE), High Gray-level Zone Emphasis (HGZE), Short Zone Low Gray-level Emphasis (SZLGE), Long Zone Low Gray-level Emphasis (LZLGE), Short Zone High Gray-level Emphasis (SZHGE), Long Zone High Gray-level Emphasis (LZHGE), Zone Percentage (ZP), Gray-level Non-Uniformity (GLNUz), Zone Length Non Uniformity (ZLNU) GLDM: Coarseness, Contrast, Busyness, Complexity, Strength
MM Granularity	Volume (Sum of intensities) η_{300} , η_{030} , η_{003}
MM Granularity Moments	Maximum, Standard deviation, Covariance, Skewness, Kurtosis, Energy, Entropy
MM Covariance	Volume (Sum of intensities) η_{300} , η_{030} , η_{003}
MM Covariance Moments	Maximum, Standard deviation, Covariance, Skewness, Kurtosis, Energy, Entropy

them separately. Among the different iterations of MM based features, significant correlations can be seen per metric. Correlations can also be noticed in some regions within the granularity and morphological covariance features showing that these features are intra-correlated.

Due to this redundancy and non-sparsity of features, PCA is used to get non-correlated features. For both the MM granularity features, the PCA coefficients are similar for all the 10 iterations, showing that there is no preference between all the initial features. However, for the MM covariance features, we observed a cycle of spikes for every 10 iterations for all the 130 iterations. This cycle is illustrated in Figure 2 for the case of volume-PCA1.

3.2 Statistical analysis

The univariate Kaplan-Meier survival analysis results for relevant features are given Table 3. After our experiments, we found that 32 features among the 159 studied are relevant to predict the survival at two years: 27 CR features and 5 MM features.

The tumor volume appears to be an important prognostic feature, as previously published in the radiomics literature [21] [22]. It appears on the fourth rank in our study with a p -value of $4.24e-5$ (Se=67%, Sp=54%, AUC=0.565 and HR=2.02). In addition to volume, two other first-order classical features are relevant: mean intensity (Se=57%, Sp=63%, AUC=0.596 and HR=1.76) and kurtosis (Se=60%, Sp=65%, AUC=0.613 and HR=1.73). Finally, 24 classical

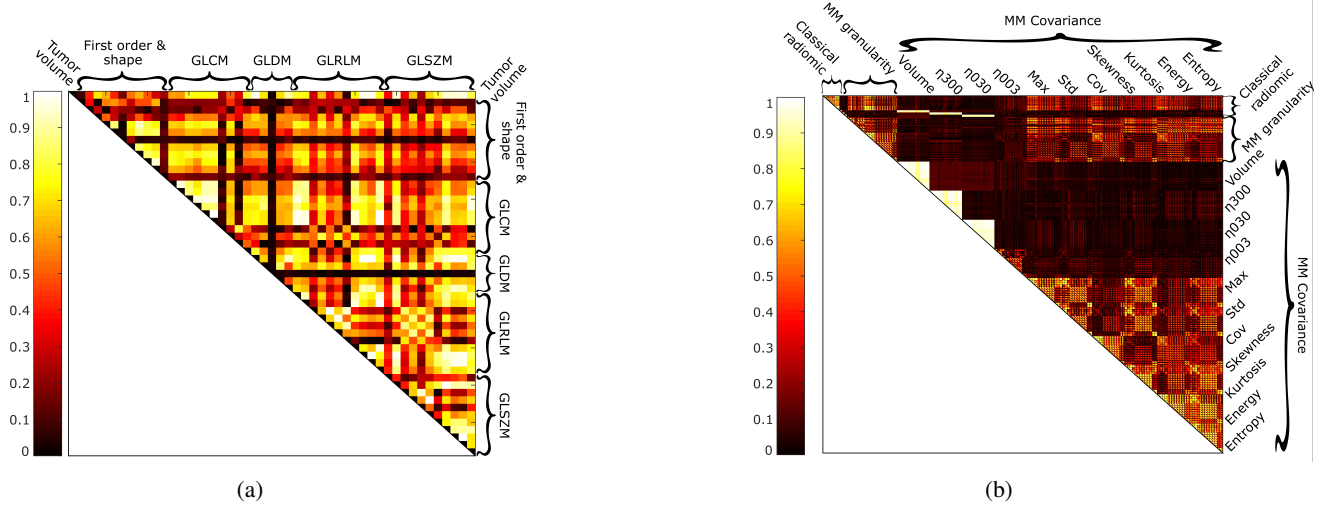


Figure 1: Matrices of Spearman's correlation absolute coefficient ($|\rho|$) (a) of the 49 classical radiomics features and (b) of all of the 1,589 studied features

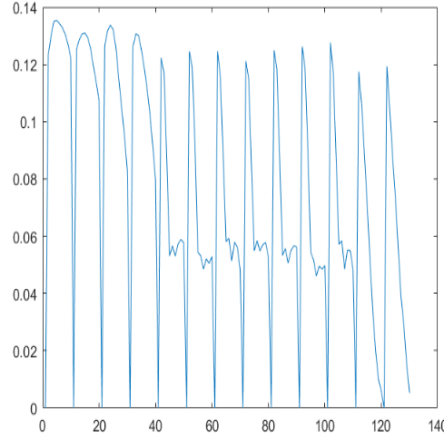


Figure 2: PCA coefficient used for the volume-PCA1 from the MM covariance.

texture features appear to have a relevant prognostic power (7 from GLCM, 8 from GLRLM, 5 from GLSZM and 4 from GLDM).

Considering the MM features, 5 of them are relevant according to survival analysis: 2 from granularity (Volume-PCA1 and Std-PCA1) and 3 from covariance (Kurtosis-PCA3, Energy-PCA2, Entropy-PCA2). We notice that none of the PCA components higher than the third rank have been selected by the statistical analysis. This means that the components with larger variance contain the relevant information. Volume-PCA1 (MM granularity) is the second most important feature of this study according to the AUC with a value of 0.631, behind strength (GLDM) (AUC=0.633), but ahead of tumor volume (AUC=0.565). Two other relevant MM features have AUC higher than 0.6, Kurtosis-PCA3 (MM Covariance) with an AUC of 0.618 and Std-PCA1 (MM granularity) with an AUC of 0.600.

In Figure 3 are given the Kaplan-Meier survival curves for six of the most interesting features. it shows that these features are able to separate the cohort into a high-risk and a low-risk group. For instance, patients having a tumor volume higher or equal to 10.53 cm³ have 2.02 times more risk to deceased (see Figure 3a). The mean survival time (OS_{mean}) for this group is 21.8 months (CI: 18-26) while it is 34.9 months (CI: 30-40) for the patients having a smaller tumor.

This observation is the same for all the relevant features. For instance, volume-PCA1 (MM granularity, Figure 3e) separates two groups of patients: one with an OS_{mean}=33.7 months (CI: 29-38) and the other with an OS_{mean}=22.1 months (CI: 18-26). The HR shows that you have 1.84 times more risk if you have a high value of this MM feature.

Table 3: List of the features with a significant prognostic power ($\alpha < 5\%$) according to the Kaplan-Meier analysis for patients with lung cancer. Sensitivity (Se), Specificity (Sp), Area Under Curves (AUC), Hazard Ratio (HR) and p -value for relevant prognostic features. CI: Confidence Interval.

Rank	Feature	Se	Sp	AUC	HR (95% CI)	p
1	GLNUz (GLSZM)	0.65	0.61	0.618	2.00 (1.51-2.66)	3.48e-5
2	Coarseness (GLDM)	0.74	0.50	0.585	2.06 (1.56-2.73)	3.48e-5
3	RP (GLRLM)	0.73	0.50	0.570	2.08 (1.57-2.74)	3.91e-5
4	Tumor volume (mL)	0.67	0.54	0.565	2.02 (1.53-2.67)	4.24e-5
5	Complexity (GLDM)	0.50	0.78	0.618	1.94 (1.43-2.63)	7.55e-5
6	GLNUr (GLRLM)	0.73	0.53	0.597	2.01 (1.52-2.66)	7.65e-5
7	Strength (GLDM)	0.70	0.56	0.633	1.93 (1.46-2.55)	1.88e-4
8	LRHGE (GLRLM)	0.43	0.74	0.568	1.89 (1.39-2.55)	2.27e-4
9	LZHGE (GLSZM)	0.81	0.37	0.591	2.02 (1.52-2.69)	3.75e-4
10	ZLNU (GLSZM)	0.76	0.46	0.597	1.92 (1.45-2.54)	5.06e-4
11	Volume-PCA1 (MM Granularity)	0.63	0.63	0.631	1.84 (1.39-2.44)	5.43e-4
12	LZE (GLSZM)	0.63	0.54	0.577	1.84 (1.39-2.44)	6.77e-4
13	SRE (GLRLM)	0.81	0.32	0.558	1.97 (1.48-2.62)	9.88e-4
14	LRE (GLRLM)	0.30	0.84	0.544	1.85 (1.32-2.58)	1.02e-3
15	Kurtosis-PCA3 (MM covariance)	0.70	0.58	0.618	1.81 (1.37-2.39)	1.69e-3
16	Energy-PCA2 (MM covariance)	0.81	0.40	0.587	1.89 (1.42-2.50)	1.73e-3
17	I_{mean}	0.57	0.63	0.596	1.76 (1.33-2.34)	1.76e-3
18	HGRE (GLRLM)	0.70	0.49	0.593	1.79 (1.35-2.36)	2.13e-3
19	Entropy (GLCM)	0.75	0.44	0.602	1.81 (1.36-2.39)	2.51e-3
20	Kurtosis	0.60	0.65	0.613	1.73 (1.31-2.29)	2.83e-3
21	SRHGE (GLRLM)	0.83	0.35	0.588	1.86 (1.40-2.48)	3.22e-3
22	RLNUr (GLRLM)	0.31	0.80	0.542	1.76 (1.26-2.44)	3.71e-3
23	Correlation (GLCM)	0.73	0.42	0.549	1.75 (1.32-2.31)	5.96e-3
24	Contrast (GLDM)	0.64	0.57	0.601	1.69 (1.28-2.24)	6.10e-3
25	Dissimilarity (GLCM)	0.36	0.81	0.596	1.69 (1.23-2.33)	8.04e-3
26	IDM (GLCM)	0.38	0.78	0.577	1.68 (1.23-2.29)	8.37e-3
27	Cluster Shade (GLCM)	0.62	0.63	0.620	1.66 (1.25-2.19)	9.31e-3
28	Entropy-PCA2 (MM covariance)	0.28	0.84	0.542	1.70 (1.22-2.38)	9.67e-3
29	Energy (GLCM)	0.43	0.77	0.588	1.65 (1.22-2.23)	9.91e-3
30	SZHGE (GLSZM)	0.80	0.32	0.557	1.77 (1.32-2.36)	1.13e-2
31	Std-PCA1 (MM Granularity)	0.62	0.55	0.600	1.64 (1.24-2.17)	0.32e-2
32	Homogeneity (GLCM)	0.36	0.79	0.578	1.65 (1.21-2.27)	1.35e-2

In addition, our experiments did not show any clinical features as relevant: p -value equal to 0.0683 for TNM stage and 0.869 for histology (both higher than 5%). On the other hand, both demographic features (age and gender) are presented as relevant: a cut-off of 68 years leads to a p -value of 0.0028 and the gender has a p -value equal to 0.0029.

4 Discussion

The role of medical imaging in clinical oncology has increased manifold in recent decades. It helps to capture intratumoral heterogeneity in a non-invasive way, which the conventional biopsy-based techniques fail to do [1]. The framework introduced in this study focused on investigating the prognostic power of MM based features extracted from CT images. By extracting both the CR and MM features, we showed the comparison between the two. To our knowledge, this is the first time MM features are studied in a radiomics analysis.

The CR features (texture based, shape based and first-order features) and MM features (granularity and morphological covariance features) are extracted from an open database of segmented NSCLC patients, captured using CT images [16]. To reduce the dimensionality and remove the redundancy of the 1,589 studied features, correlation analysis and PCA are performed. Figure 1 shows that several correlations exist between the different iterations of MM features. Hence, a PCA is performed on these features to get transformed features which are much less correlated and bring out useful information. PCA helps us to reduce the number of total features from 1,589 to 159 (49 classical radiomics features and 110 MM features). Although some work has been published on the number of PCA components that should be retained,

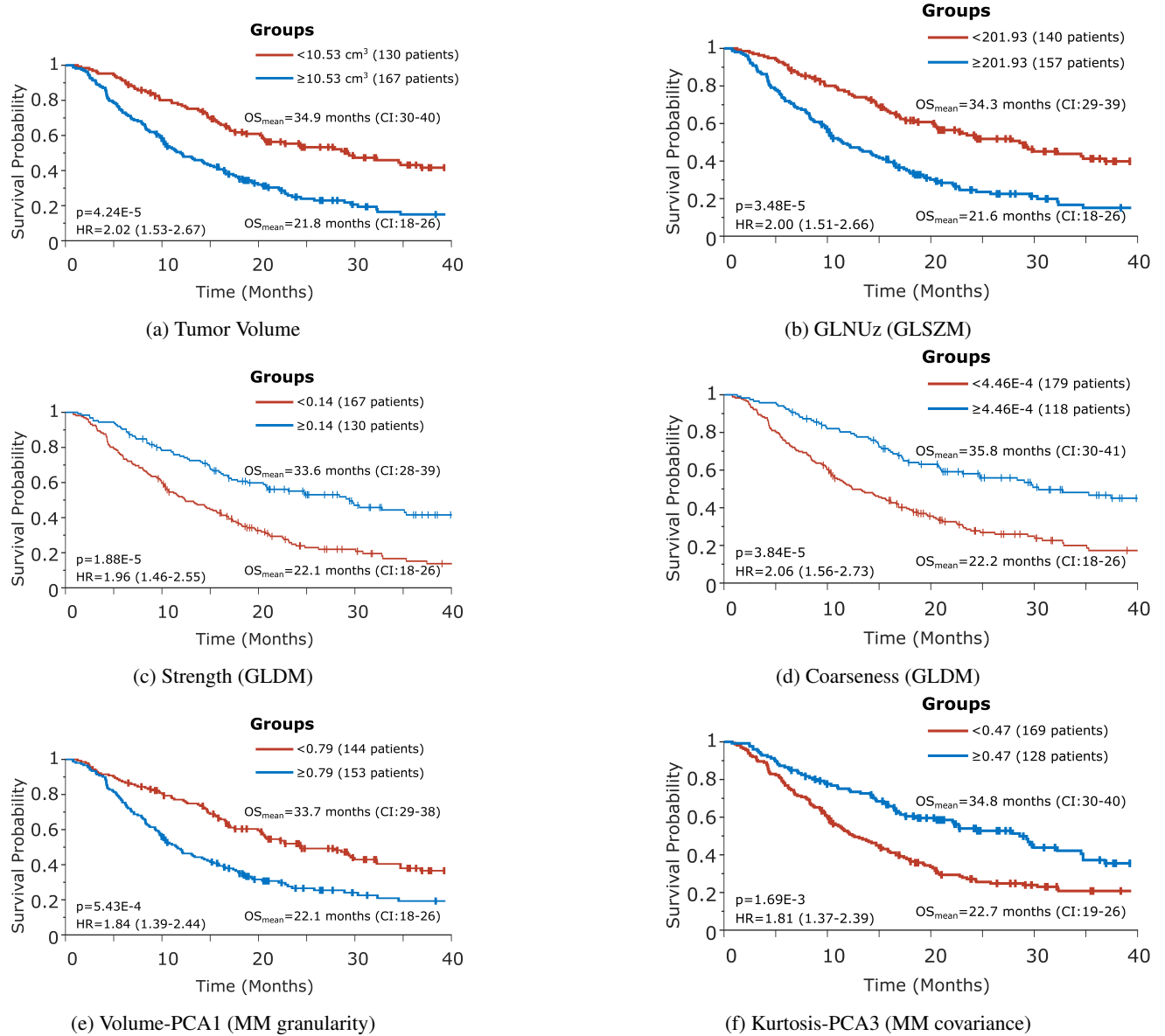


Figure 3: Kaplan-Meier survival curves.

researchers use a combination of the published rules since the results vary with the dataset used [23] [24] [25]. In this study, we retained 5 PCA components since they contained most of the information.

To analyze the prognostic power of features a Kaplan-Meier survival analysis is performed. We choose to set the horizon at two years of survival because half of the patients were deceased at this stage, making the data balanced. We found that among the 159 features studied, 32 are relevant with a p -value inferior to 5% after post-hoc corrections. Among these features, 10 have an AUC higher or equal to 0.6, out of which 7 are CR features (with Strength (GLDM) having the highest AUC of 0.633) and 3 are MM features (Volume-PCA1 and Std-PCA1 from granularity and Kurtosis-PCA3 from covariance). Among the 32 relevant features, five are MM features, proving the interest of these features to predict the survival of patients suffering from lung cancer.

The Kaplan-Meier survival curves (see Figure 3) show that relevant features successfully classify the population into high and low risk groups. Through this study, we are able to bring out new image biomarkers based on MM, to be used in survival analysis and as predictors for non invasive personalized medicine. It is also interesting to observe that the clinical features (TNM stage and histology) did not play a role in the analysis with a p -value higher to 5%.

The present study has some limitations. Because we are retrospectively studying an open source database we do not have control on all the parameters. Combining imaging data across sites leads to variations in the radiomics features and their robustness due to the use of different hardware tools, acquisition and reconstruction techniques [26]. To remove such unwanted sources of variation while preserving biological associations of interest, data harmonisation techniques are proposed in the literature such as Combat harmonization [27] [28]. Nevertheless, we were not able to use it because of the lack of knowledge about the acquisition devices used for each patient. Even though the results show that the MM features are relevant on this database, they need to be tested on other databases to establish their relevance in general. Diverse data from different databases and multiple imaging modalities can be used for further testing. We expect that using magnetic resonance imaging and PET instead of CT could bring out better results with the MM features, since these techniques are better suited for texture analysis [29] [30] [31].

5 Conclusion

In this study we investigated the prognostic power of MM based features in a radiomics study for NSCLC patients. Among the 1,589 studied features, 32 were found relevant to predict patient survival: 27 classical radiomics features and five MM features (including both granularity and morphological covariance features). These features will contribute towards the prognostic models, and eventually to clinical decision making and the course of treatment for patients.

References

- [1] Lambin P, Rios-Velazquez E, Leijenaar R, et al. Radiomics: extracting more information from medical images using advanced feature analysis. *Eur J Cancer*. 2012;48:441–446. doi: 10.1016/j.ejca.2011.11.036.
- [2] Carvalho S, Leijenaar R, Troost E, et al. 18F-fluorodeoxyglucose positron-emission tomography (FDG-PET)-Radiomics of metastatic lymph nodes and primary tumor in non-small cell lung cancer (NSCLC) - A prospective externally validated study. *PLoS ONE*. 2018;13(3):e0192859. doi: 10.1371/journal.pone.0192859.
- [3] van Timmeren J, van Elmpt W, Leijenaar R, et al. Longitudinal radiomics of cone-beam CT images from non-small cell lung cancer patients: Evaluation of the added prognostic value for overall survival and locoregional recurrence. *Radiother Oncol*. 2019;136:78-85. doi: 10.1016/j.radonc.2019.03.032.
- [4] Aerts H, Velazquez E, Leijenaar R, et al. Decoding tumour phenotype by noninvasive imaging using a quantitative radiomics approach. *Nat Commun*. 2014;5:4006. doi: 10.1038/ncomms5006.
- [5] Leijenaar R, Carvalho S, Hoebbers F, et al. External validation of a prognostic CT-based radiomic signature in oropharyngeal squamous cell carcinoma. *Acta Oncol*. 2015;54(9):1423–9. doi: 10.3109/0284186X.2015.1061214.
- [6] Aerts H, Grossmann P, Tan Y, et al. Defining a Radiomic Response Phenotype: A Pilot Study using targeted therapy in NSCLC. *Sci Rep*. 2016;6:33860. doi:10.1038/srep33860.
- [7] Coroller TP, Agrawal V, Huynh E, et al. Radiomic-Based Pathological Response Prediction from Primary Tumors and Lymph Nodes in NSCLC. *J Thorac Oncol*. 2017;12(3): 467–476. doi: 10.1016/j.jtho.2016.11.2226.
- [8] Mattonen SA. Radiomics for Response Assessment after Stereotactic Radiotherapy for Lung Cancer. Western University. 2016. <https://ir.lib.uwo.ca/etd/3926>.
- [9] Huang Y, Liu Z, He L, et al. Radiomics Signature: A Potential Biomarker for the Prediction of Disease-Free Survival in Early-Stage (I or II) Non—Small Cell Lung Cancer. *Radiology*. Radiological Society of North America; 2016;281:947–957.
- [10] Zwanenburg A, Leger S, Vallières M, et al. Image biomarker standardisation initiative. *arXiv*. 2016. <http://arxiv.org/abs/1612.07003>.
- [11] Ger R, Zhou S, Elgohari B, et al. Radiomics features of the primary tumor fail to improve prediction of overall survival in large cohorts of CT- and PET-imaged head and neck cancer patients. *PLoS ONE*. 2019;14(9):e0222509. doi:10.1371/journal.pone.0222509.
- [12] Aptoula E, Lefèvre S. Chapter 1 - Morphological Texture Description of Grey-Scale and Color Images. Hawkes PW, editor. *Advances in Imaging and Electron Physics*. Elsevier; 2011;1–74.
- [13] Thiran JP, Macq B. Morphological feature extraction for the classification of digital images of cancerous tissues. *IEEE Trans Biomed Eng*. 1996;43:1011–1020. doi: 10.1109/10.536902.
- [14] Bai X. Morphological feature extraction for detail maintained image enhancement by using two types of alternating filters and threshold constrained strategy. *Optik*. 2015;126:5038–5043. doi: 10.1016/j.ijleo.2015.09.202.

- [15] Stenning D, Lee T, van Dyk D, et al. Morphological feature extraction for statistical learning with applications to solar image data. *Statistical Analysis and Data Mining: The ASA Data Science Journal*. John Wiley & Sons, Ltd; 2013;6:329–345. doi: 10.1002/sam.11200.
- [16] Aerts H, Rios Velazquez E, Leijenaar R, et al. Data From NSCLC-Radiomics. *The Cancer Imaging Archive*. 2015. doi: 10.7937/K9/TCIA.2015.
- [17] Desbordes P, Ruan S, Modzelewski R, et al. Predictive value of initial FDG-PET features for treatment response and survival in esophageal cancer patients treated with chemo-radiation therapy using a random forest classifier. *PLoS ONE*. 2017;12(3):e0173208. doi: 10.1371/journal.pone.0173208.
- [18] Bharati M, MacGregor J. Texture analysis of images using principal component analysis. *Proc. SPIE, Process Imaging for Automatic Control*. 2001;4188:27–37. doi: 10.1117/12.417179.
- [19] Chalkidou A, O’Doherty M, Marsden P. False Discovery Rates in PET and CT Studies with Texture Features: A Systematic Review. *PLoS ONE*. 2015;4;10(5):e0124165. doi: 10.1371/journal.pone.0124165.
- [20] Altman DG, Lausen B, Sauerbrei W, et al. Dangers of using “optimal” cutpoints in the evaluation of prognostic factors. *J Natl Cancer Inst*. 1994;86:829–835. doi: 10.1093/jnci/86.11.829.
- [21] Takenaka T, Yamazaki K, Miura N, et al. The Prognostic Impact of Tumor Volume in Patients with Clinical Stage IA Non–Small Cell Lung Cancer. *J Thorac Oncol*. 2016;11(7):1074–1080. doi: 10.1016/j.jtho.2016.02.005.
- [22] Morgensztern D, Waqar S, Subramanian J, et al. Prognostic Significance of Tumor Size in Patients with Stage III Non–Small-Cell Lung Cancer: A Surveillance, Epidemiology, and End Results (SEER) Survey from 1998 to 2003. *J Thorac Oncol*. 2012;7(10):1479–1484. doi:10.1097/jto.0b013e318267d032.
- [23] Jackson DA. Stopping Rules in Principal Components Analysis: A Comparison of Heuristical and Statistical Approaches. *Ecology*. 1993;74(8):2204–2214. doi: 10.2307/1939574.
- [24] Saccenti E, Camacho J. Determining the number of components in principal components analysis: A comparison of statistical, crossvalidation and approximated methods. *Chemometrics Intellig Lab Syst*. 2015;149:99–116. doi: 10.1016/j.chemolab.2015.10.006.
- [25] Josse J, Husson F. Selecting the number of components in principal component analysis using cross-validation approximations. *Comput Stat Data Anal*. 2012;56:1869–1879. doi: 10.1016/j.csda.2011.11.012.
- [26] Mackin D, Fave X, Zhang L, et al. Measuring Computed Tomography Scanner Variability of Radiomics Features. *Investigative Radiology*. 2015;50(11):757–765. doi: 10.1097/rli.0000000000000180.
- [27] Fortin J, Parker D, Tunç B, et al. Harmonization of multi-site diffusion tensor imaging data. *Neuroimage*. 2017;161:149–170. doi: 10.1016/j.neuroimage.2017.08.047.
- [28] Fortin J, Cullen N, Sheline Y, et al. Harmonization of cortical thickness measurements across scanners and sites. *Neuroimage*. 2018;167:104–120. doi: 10.1016/j.neuroimage.2017.11.024.
- [29] Lubner M, Smith A, Sandrasegaran K, et al. CT Texture Analysis: Definitions, Applications, Biologic Correlates, and Challenges. *Radiographics*. 2017;37(5):1483–1503. doi: 10.1148/rg.2017170056.
- [30] Lu L, Ehmke R, Schwartz L, et al. Assessing Agreement between Radiomic Features Computed for Multiple CT Imaging Settings. *PLoS ONE*. 2016;11:e0166550. doi: 10.1371/journal.pone.0166550.
- [31] Shafiq-Ul-Hassan M, Zhang G, Latifi K, et al. Intrinsic dependencies of CT radiomic features on voxel size and number of gray levels. *Med Phys*. 2017;44(3):1050–1062. doi: 10.1002/mp.12123.